Relative sensitivity of photomodulated reflectance and photothermal infrared radiometry to thermal and carrier plasma waves in semiconductors

A. Salnick,[a] A. Mandelis, H. Ruda,[b] and C. Jean[c]
Photothermal and Optoelectronic Diagnostics Laboratories, Department of Mechanical and Industrial Engineering, University of Toronto, Toronto M5S 3G8, Canada

(Received 13 March 1997; accepted for publication 19 May 1997)

A quantitative theoretical comparison between two photothermal techniques—the photomodulated reflectance (PMR) and the photothermal infrared radiometry (PTR)—from the standpoint of their relative sensitivity to the thermal and carrier plasma waves in semiconductors is presented. The coefficients representing the relative contributions from the thermal and plasma waves to the total PMR and PTR signals arising as a result of the same temperature increase and photoinjected excess carrier concentration are calculated for three crystalline semiconductors: Si, Ge, and GaAs. The PTR signal is found to be extremely sensitive to the plasma-wave effects exhibiting up to five orders of magnitude higher carrier plasma-to-thermal contrast than that of the PMR method. © *1997 American Institute of Physics.* [S0021-8979(97)06316-0]

I. INTRODUCTION

In order to build a semiconductor device which provides optimal performance, it is necessary to characterize the physical properties of the semiconductor substrate and epitaxial layers before, during and after processing. Although numerous techniques have already been created and implemented into semiconductor product characterization and quality assessment instrumentation, a significant amount of work is still being directed towards the development of remote, noncontact, high-spatial-resolution methods which are capable of probing various semiconductor electronic transport properties, such as minority-carrier lifetime (τ), carrier diffusion coefficient (D_n), and surface recombination velocity (s), as well as monitoring ion implantation and impurity doping. One of the photothermal techniques, photomodulated reflectance (PMR), has progressed from a laboratory measurement method[1–6] to commercially available semiconductor inspection systems.[7,8] It was recently demonstrated that, although the PMR method is, in principle, capable of characterizing both the thermal and electronic transport parameters of semiconductor, its practical application for τ or D_n measurements is very difficult because of highly convoluted contributions from the thermal and plasma waves to the total PMR signal.[9]

Another recently established noncontact photothermal technique which has a number of potential advantages over PMR and other existing methodologies in characterization of both the thermal and electronic properties of semiconductors, is photothermal infrared radiometry (PTR).[10–16] From a rapidly growing number of experimental work on PTR detection of photoexcited carrier plasma waves in semiconductors it has become evident[10,13–15] that, unlike the PMR technique, for certain classes of materials, such as high-quality Si wafers, the plasma wave dominates the PTR signal. However, no quantitative analysis has been done yet regarding the relative sensitivity of the PMR and PTR methods to the thermal and plasma wave in semiconductors.

In this article, a quantitative theoretical comparison between these photothermal techniques is given from the point of view of their relative sensitivities to the plasma and thermal waves in crystalline semiconductors at room temperature.

II. THE PTR SIGNAL

In the PTR method the signal arises as a result of infrared emission (wavelength λ (m)) from the semiconductor due to thermal- [temperature rise $\Delta\Theta$, (K)] and plasma-wave [injected excess carrier density ΔN (m^{-3})] propagation.[10–15] It has been shown earlier[14,15] that using a classical model for wave propagation in a free plasma[17] and assuming a depth-independent IR absorption coefficient of a semiconductor $\alpha_{IR}(\lambda)$ (m^{-1}), the linear PTR signal in a one-dimensional model is

$$S_{PTR}(\omega,\alpha_{vis}) = C_T(\lambda_{vis},\Theta_0,\lambda_1,\lambda_2)\int_0^L \Delta\Theta(z;\omega,\alpha_{vis})dz + C_N(\lambda_{vis},\Theta_0,\lambda_1,\lambda_2)\int_0^L \Delta N(z;\omega,\alpha_{vis})dz \quad \text{(W)}, \tag{1}$$

where the coefficients C_T and C_N are independent of the modulation frequency $f=\omega/2\pi$ (s^{-1}), but they depend on the ambient temperature Θ_0 (K) and on the spectral range of the infrared detector λ_1 and λ_2 (m). They are given by the following expressions:

$$C_T=[1-R(\lambda_{vis})]\int_{\lambda_1}^{\lambda_2}[1-R(\lambda)]W_p(\lambda,\Theta_0)\times\frac{hc\alpha_{IR}(\lambda)d\lambda}{\lambda k_B\Theta_0^2[\exp(hc/\lambda k_B\Theta_0)-1]} \quad \left(\frac{\text{W}}{\text{mK}}\right) \tag{2}$$

and

[a]Electronic mail: salnik@mie.utoronto.ca
[b]Materials Science and Engineering Department, University of Toronto, Toronto M5S 3E4, Canada.
[c]MITEL S.C.C., 18 Boulevard de l'Aeroport, Bromont, Quebec JOE 1L0, Canada.

$$C_N=[1-R(\lambda_{\rm vis})]\int_{\lambda_1}^{\lambda_2}[1-R(\lambda)]W_p(\lambda,\Theta_0)\times\frac{\lambda^2 q^3 d\lambda}{4\pi^2 c^3 n\epsilon_0 m_{e,h}^{*2}\mu_{n,p}}\quad(\mathrm{W\,m^2}),\tag{3}$$

where $W_p(\lambda,\Theta_0)$ is Planck's distribution function:

$$W_p(\lambda,\Theta_0)=\frac{2\pi hc^2 A}{\lambda^5[\exp(hc/\lambda k_B\Theta_0)-1]}\quad\left(\frac{\mathrm{W}}{\mathrm{m}}\right).\tag{4}$$

In Eqs. (1)–(4) k_B, h, and c have their usual meanings; $\alpha_{\rm vis}$ (m^{-1}) and $R(\lambda_{\rm vis})$ are the optical absorption coefficient and reflectivity at the excitation wavelength $\lambda_{\rm vis}$(m), correspondingly, $R(\lambda)$ is the infrared reflectivity, q is the elementary charge, $m_{e,h}^*$ is the effective mass of the photoexcited minority carriers, n is the infrared refractive index, ϵ_0 is the dielectric constant of vacuum, $\mu_{n,p}$ is the mobility of minority carriers ($\mathrm{m^2/V\,s}$), $A(\mathrm{m^2})$ is the emitting surface area, and $L(\mathrm{m})$ is the semiconductor wafer thickness.

At room temperature, $\Theta_0=300$ K, and Planck's wavelength in Eq. (4) is $\lambda_p=hc/k_B\Theta_0\cong 48\ \mu$m, so that for a detector bandwidth of $\lambda_{1,2}=2-12\ \mu$m, which is typical for the HgCdTe (MCT) detector used with the PTR instrumentation,[10–16] $\exp(\lambda_p/\lambda_1)\gg\exp(\lambda_p/\lambda_2)\gg 1$. Therefore, that we can approximate in Planck's function $\exp(hc/\lambda k_B\Theta_0)-1\approx\exp(hc/\lambda k_B\Theta_0)$.

The infrared optical absorption coefficient $\alpha_{\rm IR}$ depends strongly on wavelength for doped semiconductors. In addition to the lattice absorption component, which is usually very weak for Si, Ge, and GaAs (for example, for Si at room temperature it does not exceed 100 $\mathrm{m^{-1}}$ over the 2–12 μm wavelength range),[18] for doped semiconductors there is a strong contribution due to free-carrier absorption which can be described within the Drude framework as

$$\alpha_{\rm FC}(\lambda)=\frac{\lambda^2 q^3}{4\pi^2 c^3\epsilon_0 n}\left(\frac{N_e}{m_e^{*2}\mu_n}+\frac{N_h}{m_h^{*2}\mu_p}\right),\tag{5}$$

where N_e and N_h are the concentrations of free electrons and holes, respectively.

In the near-infrared spectral range, experimentally obtained $\alpha_{\rm IR}(\lambda)$ dependencies for doped Si and Ge exhibit a $\sim\lambda^2$ behavior[19,20] and can be approximated with a good accuracy by Eq. (5) with the corresponding replacement of N_e ($\gg N_h$ for n-type materials) or N_h ($\gg N_e$ for p-type) by the product γN_i. Here $N_i(\mathrm{m^{-3}})$ is the impurity concentration and γ is the multiplying factor compensating for the difference between the absolute value of the Drude $\alpha_{\rm FC}$ and the experimental values of $\alpha_{\rm IR}$. For Si and Ge in the doping range of $N_i\sim 10^{23}-10^{26}$ $\mathrm{m^{-3}}$, the values of $\gamma_{\rm Si}=10$ (Ref. 20) and $\gamma_{\rm Ge}=4.5$ (Ref. 19) give a very good correlation between $\alpha_{\rm FC}$ and $\alpha_{\rm IR}$ in the near-infrared spectral range (1–10 μm). In the case of doped GaAs an infrared absorption coefficient exhibits a more complicated wavelength dependence $\sim\lambda^2-\lambda^{2.5}$ depending on the doping level.[21] However, assuming an estimate for the purposes of the present work, the value $\gamma_{\rm GaAs}=5\times 10^2$ gives a reasonable approximation of $\alpha_{\rm FC}$ to the experimentally observed values.[21] In principle, the exact theoretical wavelength dependencies of $\alpha_{\rm FC}$ for specific semiconductor which include all major scattering mechanisms and screening can be calculated by applying a quantum theory.[22]

In contrast to the infrared absorption, $R(\lambda)$ changes very slowly with wavelength within the range of 2–12 μm (for example, for Si these changes are less than 1%),[19,23] so that the $[1-R(\lambda)]$ term in Eqs. (2) and (3) can be taken out of the integral with $R(\lambda)$ replaced by its averaged value $\langle R_{\rm IR}\rangle$ over the detection bandwidth.

Using the foregoing assumptions, the expressions for C_T and C_N can now be rewritten as

$$C_T\cong(1-R_{\rm vis})(1-\langle R_{\rm IR}\rangle)\times\frac{h^2 q^3 A\gamma N_i}{2\pi k_B\Theta_0^2\epsilon_0 n m_{h,e}^{*2}\mu_{p,n}}\int_{\lambda_1}^{\lambda_2}\lambda^{-4}\exp\left(-\frac{2\lambda_p}{\lambda}\right)d\lambda\tag{6}$$

and

$$C_N\cong(1-R_{\rm vis})(1-\langle R_{\rm IR}\rangle)\times\frac{hq^3 A}{2\pi cn\epsilon_0 m_{e,h}^{*2}\mu_{n,p}}\int_{\lambda_1}^{\lambda_2}\lambda^{-3}\exp\left(-\frac{\lambda_p}{\lambda}\right)d\lambda.\tag{7}$$

The emitting surface area A can be approximated with a good accuracy by the area of the MCT detector (typically $1\times 1\ \mathrm{mm^2}$): $A=10^{-6}$ $\mathrm{m^2}$. Upon numerically calculating the integrals in Eq. (6) ($=3.1\times 10^{10}$ $\mathrm{m^{-3}}$) and Eq. (7) ($=4\times 10^7$ $\mathrm{m^{-2}}$) for 2–12 μm detection bandwidth, we obtain

$$C_T\cong 1.36\times 10^{-90}(1-R_{\rm vis})(1-\langle R_{\rm IR}\rangle)\frac{\gamma N_i}{n m_{h,e}^{*2}\mu_{p,n}}\quad\left(\frac{\mathrm{W}}{\mathrm{mK}}\right),\tag{8}$$

and

$$C_N\cong 1.1\times 10^{-86}\frac{(1-R_{\rm vis})(1-\langle R_{\rm IR}\rangle)}{n m_{e,h}^{*2}\mu_{n,p}}\quad(\mathrm{W\,m^2}).\tag{9}$$

Defining the ratio of the plasma-to-thermal coefficients as $\eta_{\rm PTR}$, one obtain

$$\eta_{\rm PTR}\equiv\frac{C_N}{C_T}=\frac{8\times 10^3}{\gamma N_i}\left(\frac{m_{\rm maj}^*}{m_{\rm min}^*}\right)^2\left(\frac{\mu_{\rm maj}}{\mu_{\rm min}}\right)\quad(\mathrm{m^3\,K}),\tag{10}$$

where the subscripts ''maj'' and ''min'' stand for the majority and minority carriers in a doped semiconductor, respectively.

The ratio of the plasma-to-thermal coefficients in the PTR signal is inversely proportional to the doping level, so that the highest $\eta_{\rm PTR}$ is expected for slightly doped or higher-resisitivity materials.

It should be noted, that $\eta_{\rm PTR}$ also depends on the infrared detection bandwidth, thus allowing for the unique opportunity of tuning the relative contributions from the plasma and thermal waves to the total PTR signal by varying the pair $(\lambda_1;\lambda_2)$. It can be shown that the ratio of the plasma-to-thermal coefficients in the PTR signal is decreasing with increasing λ_2 and that $\eta_{\rm PTR}$ can be changed by an order of magnitude when λ_2 is varied within the 2–24 μm near-infrared wavelength range.

TABLE I. Some optical, thermal, and electronic properties of crystalline Si, Ge, and GaAs at room temperature used for calculation of the thermal- and plasma-wave coefficients.

	Si	Ge	GaAs
Optical reflectance at $\lambda_{vis}=632$ nm, R	0.35[b]	0.48[d]	0.35[d]
Optical reflectance at $\lambda_{vis}=514$ nm, R	0.38[b]	0.50[d]	0.38[d]
Averaged IR reflectance,[a] $\langle R_{IR}\rangle$	0.50[b]	0.50[d]	0.30[d]
Impurity concentration, N_i (m^{-3})	5×10^{23}	5×10^{23}	5×10^{23}
Refractive index at $\lambda_{vis}=632$ nm, n	3.88[b]	4.60[d]	3.90[d]
Averaged IR refractive index,[a] $\langle n_{IR}\rangle$	3.42[b]	4.20[d]	3.30[d]
Electron effective mass, m_e^*/m_0	0.270[c]	0.150[c]	0.067[c]
Hole effective mass, m_h^*/m_0	0.370[c]	0.500[c]	0.082[c]
Reduced effective mass, m^*/m_0	0.156	0.115	0.037
Electron mobility, μ_n (m^2/V s)	0.150[c]	0.390[c]	0.850[c]
Hole mobility, μ_p (m^2/V s)	0.045[c]	0.190[c]	0.040[c]

[a]Over the wavelength range $\lambda=2-12$ μm.
[b]From Ref. 29.
[c]From Ref. 30.
[d]From Ref. 23.

III. THE PMR SIGNAL

As has been shown in a number of investigations devoted to the PMR technique,[3–6] The PMR signal arises from the changes of optical reflectivity ΔR of the photoexcited sample probed by the second low-power laser, as a result of both the temperature rise $\Delta\Theta$ and injected excess carrier density ΔN:

$$\Delta R=\frac{\partial R}{\partial\Theta}(\lambda_{vis},\Theta_0)\Delta\Theta(\omega,\alpha_{vis}) + \frac{\partial R}{\partial N}(\lambda_{vis},\Theta_0)\Delta N(\omega,\alpha_{vis}), \quad (11)$$

where $\Delta\Theta$ (K) and ΔN (m^{-3}) take on their surface values. Although the PMR signal is usually measured experimentally as a ratio $\Delta R/R$, for the purposes of the present work it will be kept proportional to ΔR.

In Eq. (11) the coefficient $\partial R/\partial N$ represents the contribution from the plasma wave to the total PMR signal. Generally, it has three main components[24]: the Drude or intraband component, the band-filling or interband component, and the Franz–Keldysh component due to the presence of a static electric field at a surface of a semiconductor. However, it has been shown quantitatively[24] that for crystalline semiconductors the Drude component of the coefficient $\partial R/\partial N$ is dominant and will be only considered here.

Using the weak-scattering approximation[25,26] which is valid for most of the crystalline semiconductors at visible wavelengths, the coefficient $\partial R/\partial N$ calculated within the Drude framework is[9,24]

$$\frac{\partial R}{\partial N}\cong-\frac{\lambda_{vis}^2q^2}{2\pi^2\epsilon_0m^{*2}}\frac{n-1}{n(n+1)^3}\quad(m^3), \quad (12)$$

where $m^*=m_e^*m_h^*/(m_e^*+m_h^*)$ is the effective reduced mass of the photoexcited carriers and λ_{vis} stands for the probe beam wavelength.

Although the coefficient $\partial R/\partial N$ which depends on the probe beam wavelength and the ambient temperature can, in principle, be calculated theoretically,[27] it is much more convenient to determine this parameter experimentally. In the present work the experimentally obtained values of $\partial R/\partial\Theta$ have been adopted.[9,23,24,28]

IV. COMPARISON BETWEEN PTR AND PMR

The thermal-wave coefficient C_T (PTR method) and the carrier plasma-wave coefficients C_N (PTR) and $\partial R/\partial N$ (PMR) have been calculated using Eqs. (8), (9), and (12), respectively, for the parameters listed in Table I. The values of the thermal-wave coefficient $\partial R/\partial\Theta$ have been taken from available experimental data.[9,23,28]

The results are presented in Table II along with the ratios of the carrier plasma-to-thermal coefficients η calculated for crystalline Si, Ge, and GaAs at room temperature. The PMR signal is proportional to the surface values of $\Delta\Theta$ and ΔN, Eq.(11), while in the PTR method both the temperature rise and the excess carrier concentration are integrated over the thickness of the sample, Eq.(1), so that the carrier plasma-wave and thermal-wave coefficients of both methods differ in dimensions. However, their ratios η_{PTR} and η_{PMR} have the same dimension in both methods and can be used for the comparison.

Although the carrier plasma-wave and thermal-wave coefficients presented in Table II for the PMR method are not exact and provide only order-of-magnitude accuracy as they have been calculated using the simplified Drude-theory-based model for $\partial R/\partial N$ and the experimental data for $\partial R/\partial\Theta$, they are still a very good approximation to the real values. The theoretically predicted values $\eta_{PMR}\approx7\times10^{-25}$ m^3 K for Si and $\eta_{PMR}\approx1.5\times10^{-25}$ m^3 K for Ge (Table II) are in very good agreement with the experimental results presented in Refs. 24, 27: $\eta_{PMR}\approx2\times10^{-25}$ m^3 K and $\eta_{PMR}\approx1.5\times10^{-25}$ m^3 K for Si and Ge samples, respectively. For the PTR method, an agreement between the theoretically calculated in the present work $\eta_{PTR}\sim10^{-20}$–10^{-21} m^3 K for Si with the doping level of $\sim10^{21}$ m^{-3} and the experimentally obtained $\eta_{PTR}\sim10^{-21}$ m^3 K (Ref. 15) can be considered reasonable assuming that the experimental value of η_{PTR} reported in

TABLE II. The thermal-wave ($\partial R/\partial\Theta; C_T$) and the carrier plasma-wave ($\partial R/\partial N; C_N$) coefficients and their ratios (η) in the PTR and PMR methods calculated using Eqs. (8), (9), and (12) for p- and n-type Si, Ge, and GaAs.

Parameter	p-Si	n-Si	p-Ge	n-Ge	p-GaAs	n-GaAs
$\left\vert\frac{\partial R}{\partial\Theta}\right\vert$[a], $\times 10^{-4}$ (K^{-1})	0.42[b]	0.42[b]	1.90[c]	1.90[c]	0.84[d]	0.84[d]
$\left\vert\frac{\partial R}{\partial N}\right\vert$[a], $\times 10^{-28}$ (m^3)	0.29	0.29	0.28	0.28	1.22	1.22
C_T, $\times 10^{-5}$ (W K^{-1} m^{-1})	16.9	9.5	0.45	2.52	2×10^5	1.4×10^3
C_N, $\times 10^{-25}$ (W m^2)	1.52	2.71	0.89	0.17	4.53	64.2
$\eta_{\mathrm{PMR}}=\left\vert\frac{\partial R}{\partial N}\right\vert \Big/ \left(\frac{\partial R}{\partial\Theta}\right)$, $\times 10^{-25}$ (m^3 K)	6.96	6.96	1.46	1.46	14.5	14.5
$\eta_{\mathrm{PTR}}=C_N/C_T$, $\times 10^{-22}$ (m^3 K)	9.0	28.5	193	6.67	0.02	4.54
$\eta_{\mathrm{PTR}}/\eta_{\mathrm{PMR}}$, $\times 10^3$	1.29	4.08	132	4.57	1.4×10^{-3}	0.31

[a]At $\lambda_{\mathrm{vis}}=632$ nm.
[b]From Ref. 28.
[c]From Ref. 9.
[d]From Ref. 23.

Ref. 15 has been obtained as a result of the multiparameter fitting of the PTR-amplitude and phase frequency responses and strongly depends on the choice of the other fitting parameters (s, D_n, τ).

As can be stated from the results presented in Table II, the ratio $\eta_{\mathrm{PTR}}/\eta_{\mathrm{PMR}}$ varies significantly from one semiconductor to another. For the impurity level of $N_i=5\times 10^{23}$ m^{-3}, it changes from 1.4 for p-GaAs (the lowest ratio) up to 1.3×10^5 for p-Ge (Table II). Note, that the ratio of the carrier plasma-to-thermal coefficients in the PMR method depends on the probe beam wavelength as $\sim\lambda^2$, Eq. (12), provided that the wavelength dependence of the thermal reflection coefficients is negligible. Therefore, the ratio η_{PMR} can be improved by at least an order of magnitude by changing the probe beam wavelength in the PMR method from its usual visible range (0.514–0.632 nm) to the near infrared (2–24 μm). From Eqs. (6)–(7) and (12), it is easy to see that in this case the ratio $\eta_{\mathrm{PTR}}/\eta_{\mathrm{PMR}}$ is proportional to $\sim\lambda^{-1}\exp(\lambda_p/\lambda)$ and decreases with increasing wavelength.

The ratios of the carrier plasma-to-thermal coefficients η_{PTR} and η_{PMR} represent only the relative ''weight'' of the carrier plasma-wave and the thermal-wave components in the PTR and PMR signals. In order to compare the corresponding relative sensitivities of both methods to the carrier plasma and thermal waves, we should take into account the difference in the dynamics of the photoexcited excess carriers (ΔN) and the temperature rise ($\Delta\Theta$) in the PTR and PMR methods, Eqs. (1) and (11).

Assuming for a highly absorbing semi-infinite semiconductor the temperature and free-carrier fields to be

$$\Delta\Theta(z)=\frac{(h\nu-E_g)I_0}{h\nu k\sigma_t}\,e^{-\sigma_t z}\quad (\mathrm{K}), \tag{13}$$

and

$$\Delta N(z)=\frac{I_0}{h\nu(D_n\sigma_n+s)}\,e^{-\sigma_n z}\quad (\mathrm{m}^{-3}), \tag{14}$$

where I_0 (W/m^2) is the excitation power density, $h\nu$ (J) is the photon energy, E_g (J) is the semiconductor band gap, k (W/m K) is the thermal conductivity, D_n and β(m^2/s) are the minority carrier and thermal diffusivities, respectively, s (m/s) is the surface recombination velocity, τ(s) is the minority-carrier lifetime, and the magnitudes of the complex thermal- and plasma-wave vectors are defined as

$$\sigma_t^2=\frac{i\omega}{\beta};\quad \sigma_n^2=\frac{1+i\omega\tau}{D_n\tau}, \tag{15}$$

the PTR and PMR signals, Eqs. (1) and (11) can be written as

$$S_{\mathrm{PTR}}(\omega)=C_T\,\frac{(h\nu-E_g)I_0}{h\nu k\sigma_t^2}+C_N\,\frac{I_0}{h\nu\sigma_n(D_n\sigma_n+s)}\quad (\mathrm{W}) \tag{16}$$

and

$$S_{\mathrm{PMR}}(\omega)=P_W\left(\frac{\partial R}{\partial\Theta}\right)\frac{(h\nu-E_g)I_0}{h\nu k\sigma_t}-P_W\left\vert\frac{\partial R}{\partial N}\right\vert\frac{I_0}{h\nu(D_n\sigma_n+s)}\quad (\mathrm{W}), \tag{17}$$

where P_W (W) is the probe beam power in the PMR method.

Defining the carrier plasma-to-thermal contrast ξ as a ratio of the plasma to thermal terms in Eqs. (16) and (17) $\xi=\vert S_{\mathrm{plasma}}\vert/\vert S_{\mathrm{thermal}}\vert$, we obtain

$$\xi_{\mathrm{PTR}}=\eta_{\mathrm{PTR}}\,\frac{k\sigma_t^2}{(h\nu-E_g)\sigma_n(D_n\sigma_n+s)} \tag{18}$$

and

$$\xi_{\mathrm{PMR}}=\eta_{\mathrm{PMR}}\,\frac{k\sigma_t}{(h\nu-E_g)(D_n\sigma_n+s)}. \tag{19}$$

These ratios represent the relative sensitivity of the PTR and PMR methods to carrier plasma and thermal waves in

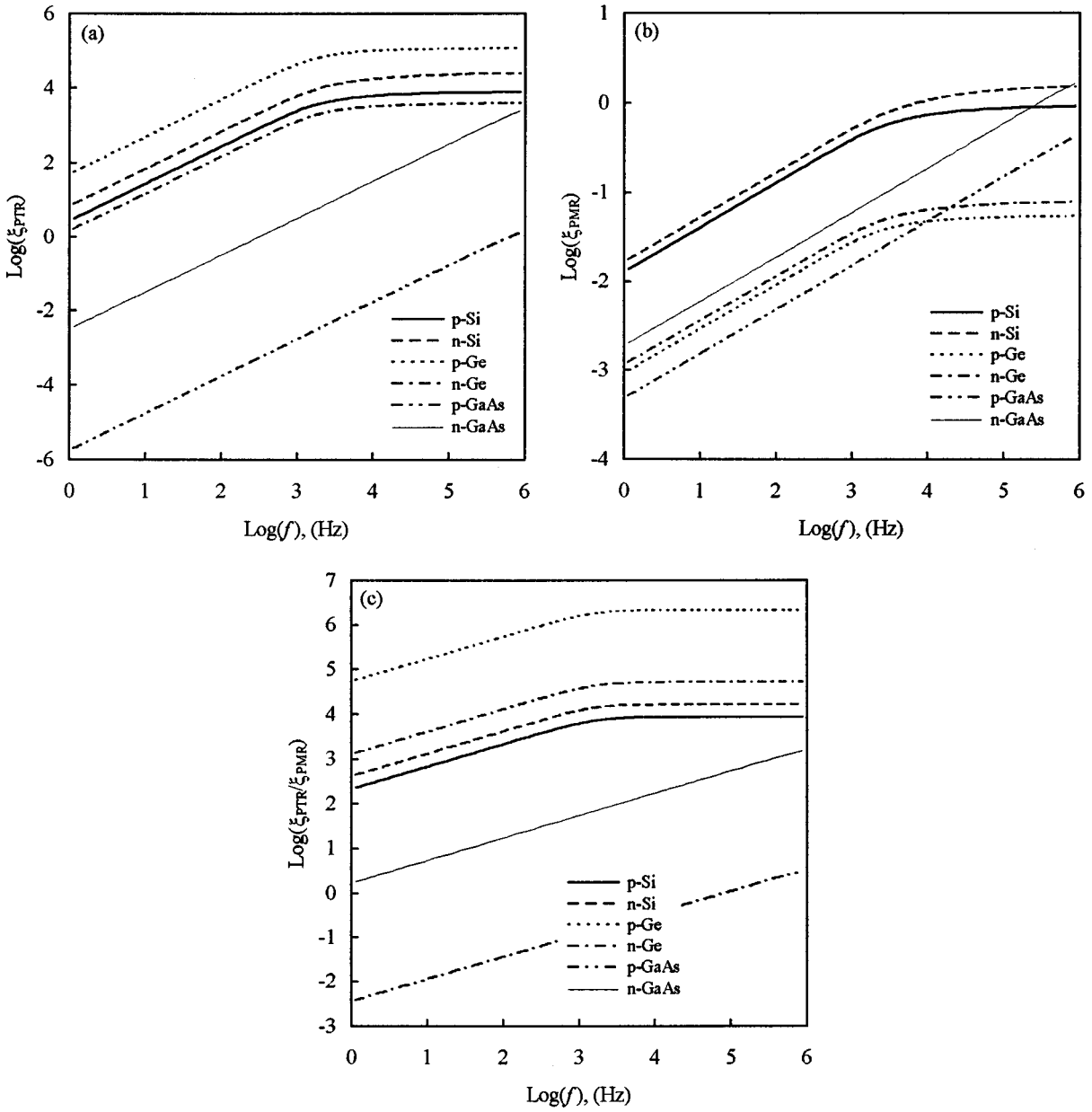

FIG. 1. Carrier plasma-to-thermal contrast factors (ξ) of the (a) PTR and (b) PMR signals and their ratio (c) as a functions of modulation frequency for Si, Ge, and GaAs of both types of conductivity calculated using Eqs. (16) and (17) and the η values of Table II. The sets of [D_n(m^2/s); τ (s); β(m^2/s); s(m/s)] values used for the calculations are as follows: p-Si(3.5×10^{-3};10^{-4};8×10^{-5},5), n-Si(1.2×10^{-3};10^{-4};8×10^{-5},5), p-Ge(9.1×10^{-3};10^{-4};3.6×10^{-5},5), n-Ge(4.4×10^{-3};10^{-4};3.6×10^{-5},5), p-*GaAs*(1.98×10^{-2};10^{-7};2.4×10^{-5},10), n-GaAs(1.1×10^{-3};10^{-7};2.4×10^{-5},10).

semiconductors for one-dimensional geometry and can be used to determine the regions of plasma-wave ($\xi\gg1$) and thermal-wave ($\xi\ll1$) domination in both methods.

Finally, for the ratio of the carrier plasma-to-thermal contrasts of the PTR and PMR methods we obtain the following simple relation:

$$\frac{\xi_{\mathrm{PTR}}}{\xi_{\mathrm{PMR}}}=\left(\frac{\eta_{\mathrm{PTR}}}{\eta_{\mathrm{PMR}}}\right)\left(\frac{\sigma_t}{\sigma_n}\right). \tag{20}$$

The ratio of the plasma-to-thermal contrasts is proportional to the previously described ratio $\eta_{\mathrm{PTR}}/\eta_{\mathrm{PMR}}$ and depends on the carrier plasma and thermal wave dynamics, thus the PTR and PMR method relative sensitivities should be compared on a modulation frequency scale.

Figure 1 represents the carrier plasma-to-thermal contrasts of the PTR and PMR signals along with their ratios as functions of modulation frequency for six different semiconductor materials considered in the present work. As can be seen, for Si and Ge the PTR signal is dramatically dominated by the plasma-related effects over the entire frequency range used for the simulation (1 Hz–1 MHz) and for the choice of the typical thermal and electronic transport parameters listed in the caption. The plasma-to-thermal contrast here is saturated at high frequencies at the level of $\sim10^4$ [Fig. 1(a)].

For GaAs the PTR signal behavior changes from thermal domination at low frequencies to plasma domination at high frequency in the case of n-GaAs. The PTR signal contrast,

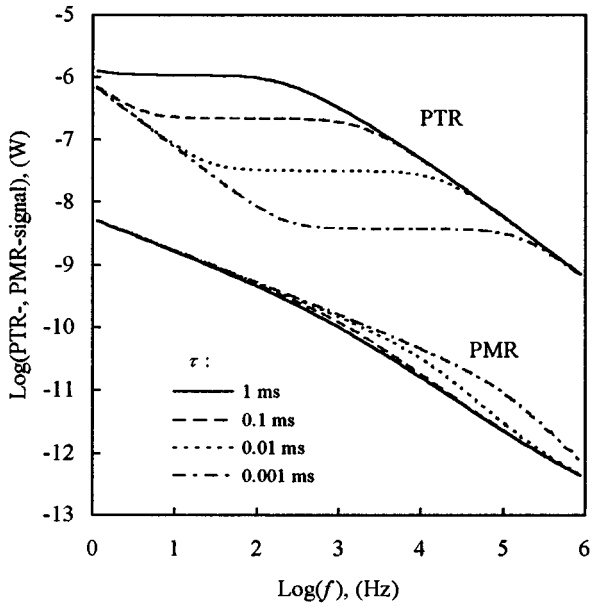

FIG. 2. PTR and PMR amplitude frequency responses for p-Si calculated using the values of the carrier plasma-wave and thermal-wave coefficients of Table II with different minority-carrier lifetimes, as indicated in the insets. Other calculating parameters are: $h\nu=2.41$ eV, $I_0=10^4$ W/m^2, $N_i=5\times10^{24}$ m^{-3}, $E_g=1.12$ eV, $D_n=3.5\times10^{-3}$ m^2/s, $s=5.0$ m/s, $k=150$ W/m K, and $\beta=8\times10^{-5}$ m^2/s.

however, remains thermally dominated over the entire frequency range for p-GaAs.

As has been expected from the comparison of the η ratios of Table II, the PMR signal for the same samples is thermally dominated with a tendency of equalizing the relative contributions from the thermal and plasma waves at high frequencies for p-Si and p-Ge [Fig. 1(b)].

The comparison of the relative sensitivities of the PTR and PMR signals presented in Fig. 1(c) as the ratio $\xi_{\mathrm{PTR}}/\xi_{\mathrm{PMR}}$ clearly shows a higher (up to six orders of magnitude) sensitivity of the PTR method to the plasma-related effects than that of the PMR for Si, Ge and n-GaAs samples in the frequency range $1-10^6$ Hz.

In order to illustrate how the foregoing difference in plasma-to-thermal contrasts affects the relative sensitivity of measured PTR and PMR signals to changes in carrier lifetimes, in Fig. 2 the amplitude frequency responses of both methods are simulated, assuming the typical experimental parameters listed in figure caption.

The quantitative character of the calculations in the present work allows the comparison of not only the relative frequency behavior of the PTR and PMR amplitudes, but also of an absolute magnitude for both signals. The PTR amplitude is proportional to the surface emitting area $S_{\mathrm{PTR}}\sim A$ (typical value of 1×1 mm^2 is assumed) and the magnitude of the PMR signal is a linear function of the probe beam power: $S_{\mathrm{PMR}}\sim P_W$ (taken to be 1 mW).

For a p-Si sample with $N_i=5\times10^{24}$ m^{-3}, the plasma-dominated PTR signal is nearly two orders of magnitude stronger than the corresponding thermally-dominated PMR amplitude response for $\tau>10\,\mu$s (Fig. 2). As has been shown theoretically and experimentally,[10,13–15] in the PTR method the thermal- and the carrier plasma-wave components are well separated in the frequency scale and the PTR amplitude frequency response consists of three characteristic regions: a thermally-dominated low-frequency part with $\sim\omega^{-1}$ dependence, an intermediate frequency plateau with a level proportional to the carrier lifetime for the samples with low s, and a plasma-dominated high-frequency region exhibiting a frequency behavior between $\sim\omega^{-1}$ and $\sim\omega^{-0.5}$ for low and high S.

Unlike the PTR signal, the PMR amplitude frequency responses do not show any significant sensitivity for three orders-of-magnitude variations in the carrier lifetime, with the PMR amplitude being only slightly affected by τ at high frequencies (Fig. 2).

In conclusion, the present work shows that the PTR method is extremely sensitive to the plasma-wave effects in crystalline semiconductors exhibiting in one-dimensional geometry (well represented for pump laser spot sizes $\geqslant50\,\mu$m) up to five orders of magnitude higher carrier plasma-to-thermal contrast than that of the conventional PMR method. Although the plasma-to-thermal contrast of the PMR signal can be improved, in principle, by increasing the excitation power density, different associated undesirable effects such as non-linear recombination[31,32] or the necessity to account for a full coupling between the thermal and plasma waves[16] may render the interpretation of the PMR experimental results very difficult.

ACKNOWLEDGMENTS

The support of the Natural Sciences and Engineering Research Council of Canada (NSERC) through a Collaborative Project Grant is gratefully acknowledged. One of the authors (A.S.) is also grateful to NSERC for a NATO Science Research Fellowship Award.

[1] E. Y. Wang, W. A. Albers, and C. E. Bleil, in *II-VI Semi-Conducting Compounds*, edited by R. Thomas (Benjamin, New York, 1967), p. 136.
[2] A. M. Bonch-Bruevich, V. P. Kovalev, G. S. Romanov, Y. A. Imas, and M. N. Libenson, Sov. Phys. Tech. Phys. **13**, 507 (1968).
[3] J. Opsal and A. Rosencwaig, Appl. Phys. Lett. **47**, 498 (1985).
[4] A. Rosencwaig, in *Photoacoustic and Thermal-Wave Phenomena in Semiconductors*, edited by A. Mandelis (Elsevier, New York, 1987), Chap. 5.
[5] C. Christofides, I. A. Vitkin, and A. Mandelis, J. Appl. Phys. **67**, 2815 (1990).
[6] A. Vitkin, C. Christofides, and A. Mandelis, J. Appl. Phys. **67**, 2822 (1990).
[7] Therma-Probe™ series, Therma-Wave Inc. (Fremont, CA).
[8] Thermal Wave Module™ series, Jenoptik Carl Zeiss Jena GmbH (Jena, Germany).
[9] A. Mandelis and R. Wagner, Jpn. J. Appl. Phys. **35**, 1786 (1996).
[10] J. Sheard, M. G. Somekh, and T. Hiller, Mater. Sci. Eng. B **5**, 101 (1990).
[11] Z. H. Chen, R. Bleiss, A. Mandelis, and F. Shimura, J. Appl. Phys. **73**, 5043 (1993).
[12] A. Mandelis, R. Bleiss, and F. Shimura, J. Appl. Phys. **74**, 3431 (1993).
[13] A. Salnick, A. Mandelis, and C. Jean, Appl. Phys. Lett. **69**, 2522 (1996).
[14] A. Salnick, C. Jean, and A. Mandelis, Solid-State Electron. **41**, 591 (1997).
[15] A. Mandelis, A. Othonos, C. Christofides, and J. Boussey-Said, J. Appl. Phys. **80**, 5332 (1996).
[16] A. Mandelis, M. Nestoros, and C. Christofides, Opt. Eng. (Bellingham) **36**, 459 (1997).
[17] S. Ramo, J. R. Whinnery, and T. Van Duzer, *Fields and Waves in Communication Electronics* (Wiley, New York, 1965), p. 334.

[18] F. A. Johnson, Proc. Phys. Soc. **73**, 265 (1959).
[19] R. A. Soref and B. R. Bennett, IEEE J. Quantum Electron. **QE-23**, 123 (1987).
[20] H. Y. Fan, W. Spitzer, and R. J. Collins, Phys. Rev. **101**, 566 (1956).
[21] K. Osamura and Y. Mirakami, Jpn. J. Appl. Phys. **11**, 365 (1972).
[22] H. Ruda, J. Appl. Phys. **61**, 3035 (1987).
[23] A. Dargys and J. Kundrotas, *Handbook of Physical Properties of Ge, Si, GaAs and InP* (Science and Encyclopedia Publishers, Vilnius, 1994), Chaps. 1–3.
[24] R. E. Wagner, Ph.D. thesis, University of Toronto, Toronto, 1994.
[25] W. A. Harrison, *Solid State Theory* (Dover, New York, 1979), p. 287.
[26] G. E. Carver and J. D. Michalski, Proc. SPIE **794**, 152 (1987).
[27] R. Wagner and A. Mandelis, J. Phys. Chem. Solids **52**, 1061 (1991).
[28] G. E. Jellison, Jr. and H. H. Burke, J. Appl. Phys. **60**, 841 (1986).
[29] *Properties of Silicon*, EMIS Datareviews Series No. 4 (INSPEC, The Institution of Electrical Engineers, London, 1988), pp. 72–79.
[30] M. Sze, *Physics of Semiconductor Devices*, 2nd ed. (Wiley, New York, 1981), p. 850.
[31] R. E. Wagner and A. Mandelis, Semicond. Sci. Technol. **11**, 289 (1996).
[32] R. E. Wagner and A. Mandelis, Semicond. Sci. Technol. **11**, 300 (1996).